We are IntechOpen, the world's leading publisher of Open Access books Built by scientists, for scientists

4,800
Open access books available

122,000
International authors and editors

135M
Downloads

Our authors are among the

154
Countries delivered to

TOP 1%
most cited scientists

12.2%
Contributors from top 500 universities

CLARIVATE ANALYTICS BOOK CITATION INDEX INDEXED

WEB OF SCIENCE™

Selection of our books indexed in the Book Citation Index in Web of Science™ Core Collection (BKCI)

Interested in publishing with us?
Contact book.department@intechopen.com

Numbers displayed above are based on latest data collected.
For more information visit www.intechopen.com

15

Simulation of H_2-Air Non-Premixed Flame Using Combustion Simulation Technique to Reduce Chemical Mechanisms

Kazui Fukumoto and Yoshifumi Ogami
Ritsumeikan University, 1-1-1 Noji-Higashi, Kusatsu, Shiga
Japan

1. Introduction

Combustion simulation that uses computational fluid dynamics (CFD) has been widely adopted as the design tool for combustion equipment. Because flow inside such equipment is generally turbulent, turbulence and combustion models are needed to simulate combustion; many combustion simulations have been performed to verify a system's internal state, such as velocity, pressure, mole fractions of chemical species, and temperature.

Combustion simulation of a confined impinging jet reactor has been performed by the large eddy simulation (LES) model serving as the turbulence model and the presumed probability density function (PDF) serving as the combustion model (Daniele, 2009). The analysis shows that a confined impinging jet reactor is indeed an interesting device because of its high mixing efficiency and absence of stagnant and recirculation zones.

Under the condition of moderate or intense low-oxygen dilution (MILD), the effect of H_2 on H_2-CH_4 turbulent non-premixed flames was investigated with the improved standard $k-\epsilon$ model as the turbulence model and with the eddy dissipation concept (EDC) model (Amir et al., 2010). Simulation results show that H_2 addition to CH_4 leads to improved mixing, increase in turbulent kinetic energy decay along the flame axis, increase in flame entrainment, higher reaction intensities, and increase in mixture ignitability and rate of heat release.

Although combustion simulation was considered to be an efficient designing tool, considerable computational time was needed to calculate the chemical reaction. Combustion models that detail chemical mechanisms require reaction calculations involving n-dimensional ordinary differential equations (ODEs) that are solved according to the number of chemical species involved. Therefore, reducing computation time for the combustion simulation is a significant problem. If computation time could be easily reduced according to the required prediction accuracy, we would be able to obtain the results more quickly. For example, O is a significant species whose mass fraction is necessary to compute the amount of NO present; therefore, the accuracy of the mass fraction of O cannot be neglected. To determine this mass fraction with sufficient accuracy, it is necessary to build a reduced mechanism including O. Generally, a quasi-steady state or partial equilibrium is assumed when the reduced mechanism is built (Warrants et al., 2006).

The chemical equilibrium method (Nagai et al., 2002) does not use reaction equations; instead, the equilibrium composition of a chemical system is determined by minimizing the

Gibbs free energy, which is subject to the conservation of the chemical elements involved in the combustion. The composition is obtained by solving a system of simultaneous nonlinear equations with five unknowns (one for each of the elemental species involved in that study, namely, C, H, O, and N, plus one). In another study, a partial non-premixed flame of CH_4 was modeled using the vortex method in combination with the chemical equilibrium method (Ogami et al., 2010). Although this method did not use any chemical equations, the calculated temperature and main products were in good agreement with experimental results. In some cases, the data obtained from the simulation concerning the minor products did not agree with the experimental results.

A combustion simulation technique based on a combination of the chemical equilibrium method and the EDC model was developed in a previous study and validated by simulation of a H_2-air turbulent non-premixed flame (Fukumoto et al., 2010) and a CO-H_2-air turbulent non-premixed flame (Fukumoto et al., 2009). An advantage of the technique is the ease with which a reduced chemical mechanism can be built according to the accuracy requirement for the chemical species. Thus, the technique can predict intermediate species with high accuracy when a reduced mechanism for the minor species is built. The key to this proposed technique is the incorporation of the concept of equilibrium into the chemical kinetics, which decreases the dimensionality of the chemical reaction calculation and reduces the computational time for a combustion simulation.

This chapter presents a technique for combustion simulation based on a chemical equilibrium method and an EDC model (Magnussen, 1989, 2005). The advantage of the proposed technique is that it makes it easy for us to construct a reduced mechanism according to the accuracy requirements of the chemical species. The proposed technique is validated through a simulation of a H_2-air non-premixed flame (Barrow et al., 2003a). The results computed using the proposed technique are then compared with experimental data and computational data obtained by the EDC model.

2. Method

Ansys FLUENT version 13.0 (Ansys, Inc., 2011) was used in this study. The temperature, enthalpy, and reaction rate of the chemical species were calculated by a user-defined function (UDF) in FLUENT. The UDF is a function that can be programmed to load dynamically with the FLUENT solver in order to enhance the standard features of FLUENT. Moreover, the momentum equation, turbulence model, and mass fraction equation were computed using Ansys FLUENT.

To solve the momentum equation, velocity and pressure were coupled by the SIMPLE method; the basic Reynolds stress model with a function of the enhanced wall treatment in Ansys FLUENT (Ansys, Inc., 2010) was chosen as the turbulence model. The temperature was obtained by computation of the following energy equation:

$$\frac{\partial(\bar{\rho}\tilde{u}_i\tilde{h})}{\partial x_i} = -\frac{\partial}{\partial x_i}\left(\bar{q}_J + \bar{\rho}\overline{u_i'h'}\right) + \bar{q}_{\mathrm{rad}}, \tag{1}$$

$$\bar{\rho}\overline{u_i'h'} = -\frac{\mu_t}{\sigma_h}\frac{\partial\tilde{h}}{\partial x_i}, \tag{2}$$

$$\bar{q}_J = -\lambda \frac{\partial \bar{T}}{\partial x_i}, \tag{3}$$

where $\bar{\rho}$ represents the density, $\tilde{u}_i$ represents the gas velocity of i components, $\tilde{h}$ is the enthalpy, $\bar{q}_{\mathrm{rad}}$ is the source term of the radiation, x_i is the coordinate in the i direction, μ_t is the turbulent viscosity, σ_h is the effective Prandtl number, λ is the heat conductivity, and $\bar{T}$ is the temperature. The symbols "~" and "–" placed over the variables indicate density weighted and time average, respectively. $\bar{q}_{\mathrm{rad}}$ was modeled as described on the TNF web site (Barrow, 2003b), and $\bar{T}$ was computed as

$$\bar{T} = T_0 + \frac{\tilde{h} - \sum_J \tilde{Y}_J h_{J0}}{Cp_J}, \tag{4}$$

where $T_0 = 298.15$. h_{J0} represents the standard enthalpy of the formation of chemical species J, $\tilde{Y}_J$ is the mass fraction of chemical species J, and Cp_J is the mean specific heat at constant pressure of chemical species J.

2.1 Combustion simulation technique

The proposed technique is explained using the example of a H_2-air turbulent non-premixed flame. Figure 1 illustrates the scheme of the proposed technique. In this technique, chemical species are divided, roughly, into two groups: group a—the species categorized by the chemical equilibrium, and group b—the species categorized by the chemical kinetics (including the overall reaction).

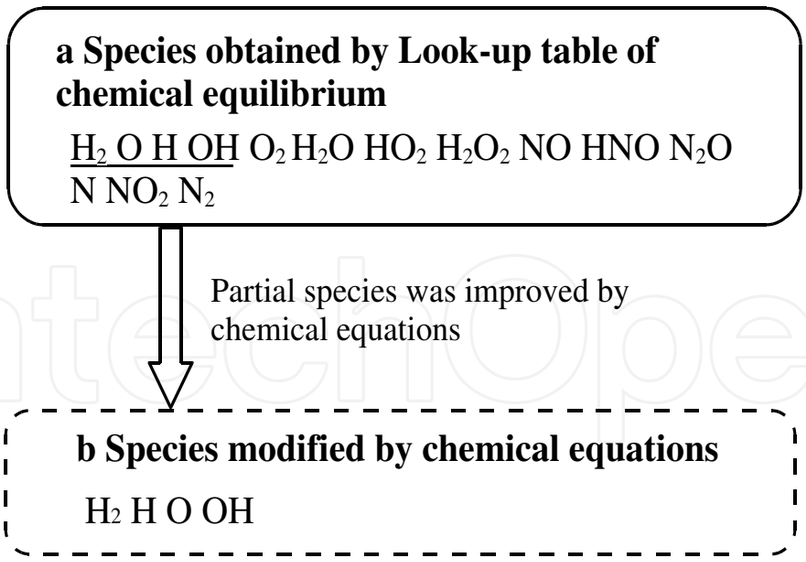

Fig. 1. Overview of proposed technique

In the proposed technique, the mass fraction equation of chemical species J was used as

$$\frac{\partial}{\partial x_j}(\bar{\rho}\tilde{u}_j\tilde{Y}_J) = -\frac{\partial}{\partial x_j}\left(\bar{j}_{jJ} + \bar{\rho}\overline{u_j'Y_J'}\right) + \bar{w}_J, \tag{5}$$

$$\overline{j}_{jJ} = -\overline{\rho} D_J \frac{\partial \tilde{Y}_J}{\partial x_j}, \tag{6}$$

$$\overline{\rho}\overline{u_j}Y_J' = -\frac{\mu_t}{\sigma_m}\frac{\partial \tilde{Y}_J}{\partial x_i}, \tag{7}$$

where $\overline{w}_J$ represents the reaction rate of chemical species J; D_J, the effective diffusion coefficient of chemical species J; and σ_m, the effective Schmidt number. The eddy dissipation concept (Magnussen, 1989; Gran et al., 1996; Magnussen, 2005) was used to model $\overline{w}_J$, and D_J was estimated using Smooke's model. To obtain $\overline{w}_J$ in Equation (5), calculations of the chemical reaction and chemical equilibrium were performed; the mass fraction equation can be computed by assignment of a value to $\overline{w}_J$.

To perform the chemical equilibrium calculation, we needed the mass fraction of elemental species I and enthalpy in group b. We therefore added the mass fraction equation of elemental species J in group a:

$$\frac{\partial(\overline{\rho}\tilde{u}_j\tilde{Z}_I)}{\partial x_j} = \frac{\partial}{\partial x_j}\left(\frac{\mu_t}{\sigma_m}\frac{\partial \tilde{Z}_I}{\partial x_i}\right) + \overline{w}_I, \tag{8}$$

where $\tilde{Z}_I$ represents the mass fraction of elemental species I. $\overline{w}_I$ is the source term that exchanges the mass in group b for that in group a:

$$\overline{w}_I = -M_I\left[\sum_{J_\mathrm{b}} \frac{a_{IJ_\mathrm{b}}\overline{w}_{J_\mathrm{b}}}{M_{J_\mathrm{b}}}\right], \tag{9}$$

where M_I represents the atomic weight of species I, J_b the chemical species J in group b, a_{IJ_b} the number of elemental species I included in chemical species J_b, $\overline{w}_{J_\mathrm{b}}$ the reaction rate of chemical species J_b, and M_{J_b} the mole weight of chemical species J_b.

The enthalpy in group a was approximated as

$$\tilde{h}_\mathrm{a} = \tilde{h}\sum_I \tilde{Z}_I, \tag{10}$$

where $\tilde{h}_\mathrm{a}$ represents the enthalpy in group a.

The source term in Equation (5) for the equilibrium species J_a was modeled as

$$\overline{w}_{J_\mathrm{a}} = \frac{\overline{\rho}(\xi^*)^2}{\tau^*}(Y_{J_\mathrm{aeq}} - Y_{J_\mathrm{a}}^0), \tag{11}$$

where J_a is the chemical species J in group a, $\overline{w}_{J_\mathrm{a}}$ is the reaction rate of chemical species J_a, ξ^* is the fine scale, τ^* is the time scale of the reaction, and Y_{J_aeq} is the mass fraction of chemical species J_a obtained from the lookup table, which was prepared before the combustion simulation. The lookup table stored the results of the chemical equilibrium calculation when $\tilde{Z}_I$ and $\tilde{h}_\mathrm{a}$ were varied, and these values were also used to extract the equilibrium values from the lookup table.

$Y_{J_\mathrm{a}}^0$ in Equation (11) was estimated as

$$\tilde{Y}_J = \xi^3 Y_J^* + (1.0 - \xi^3) Y_J^0. \tag{12}$$

where J indicates J_a.

ξ^* was modeled as

$$\xi^* = C_\xi \left(\frac{\mu\epsilon}{\bar{\rho}k^2} \right)^{1/4}, \tag{13}$$

where $C_\xi = 2.1377$. μ represents the viscosity, ϵ the turbulent dissipation rate, and k the turbulent kinetic energy. τ^* was given as

$$\tau^* = C_\tau \left(\frac{\mu}{\bar{\rho}\epsilon} \right)^{1/2}, \tag{14}$$

where $C_\tau = 0.408$.

The proposed technique was needed to compute $\bar{w}_J$ in Equation (5), and different expressions were used to compute $\bar{w}_J$, depending on the group that the species belonged to. The reaction rate of chemical species in group b can be obtained with the EDC model. The source term in Equation (5) for these modified chemical species was computed as

$$\bar{w}_{J_b} = \begin{cases} \dfrac{\bar{\rho}(\xi^*)^2}{\tau^*} \left[\max(Y_{J_b}^* - Y_{J_b}^0, Y_{J_{beq}}) \right], & (Y_{J_b}^* - Y_{J_b}^0 \geq 0.0) \\ \dfrac{\bar{\rho}(\xi^*)^2}{\tau^*} \left[Y_{J_b}^* + Y_{J_{beq}} - Y_{J_b}^0 \right], & (Y_{J_b}^* - Y_{J_b}^0 < 0.0), \end{cases} \tag{15}$$

where $\bar{w}_{J_b}$ represents the reaction rate in group b; $Y_{J_b}^*$, the chemical species J_b in the fine structures; $Y_{J_b}^0$, the chemical species J_b in the surrounding gas; and $Y_{J_{beq}}$, the mass fraction of the chemical species J_b obtained from the lookup table.

Since the lookup table included the mass fraction of the chemical species in group b, the production resulting from using the values take from the table must be taken into account. When $Y_{J_{beq}} = 0$, these equations were similar to what was seen in the EDC model.

$Y_{J_b}^*$ was obtained by calculating the detailed chemical mechanism. The EDC model assumes that combustion occurs in a constant pressure reactor. The following equation was integrated under the initial conditions obtained from the current mass fractions, density, and temperature in each computational cell:

$$\frac{dY_{J_b}^*}{dt} = \frac{w_{J_b}^*}{\rho}, \tag{16}$$

where $w_{J_b}^*$ represents the reaction rate of chemical species J_b in the fine structures, and $w_{J_b}^*$ can be obtained by computing detailed chemical mechanisms based on the Arrhenius equation. Equation (16) is a stiff ODE, and therefore, the robust computational code CVODE (Hindmarsh et al., 2009) was used to acquire the steady solution.

Although the reaction rates of fuels can be computed by Equation (15), the flame sometimes blows out. That is why we used the following equations to estimate the reaction rates of the

fuels in this study. If we assumed that the reaction rates of fuels were determined with an overall reaction such as $1(\text{kg})\text{fuel} + st(\text{kg})\text{oxidant} \Rightarrow (1+st)(\text{kg})\text{products}$, Y_{fu}^{*} can be modeled based on the expression of the overall reaction rate as

$$Y_{\text{fu}}^{*} = \tilde{Y}_{\text{fu}} - \Delta Y_{\text{fu}} \tag{17}$$

$$\Delta Y_{\text{fu}} = A_{\text{fu}} \min(\tilde{Y}_{\text{fu}}, \frac{\tilde{Y}_{\text{ox}}}{st}). \tag{18}$$

The subscripts fu and ox represent the fuels and oxidants, respectively. st represents the theoretical weight of the oxidants, and A_{fu} is the mixing parameter of fuels set to 1.0 (equal to the value in the original EDC model).

2.2 Chemical equilibrium method and reading lookup table

When preparing the lookup table, we developed a different program from the UDF based on the chemical equilibrium method, by minimization of the Gibbs free energy. This method assumes that the equilibrium composition of a chemical system can be determined by minimizing the Gibbs free energy. Under the minimum conditions of Gibbs free energy, the following simultaneous nonlinear equations are obtained:

$$X_0 \sum_J a_{IJ} \exp\left[-\sum_K \frac{\alpha_{KJ}\beta_I}{RT} - \left(\frac{G_J}{RT} + \ln p \right) \right] = d_I, \tag{19}$$

$$\sum_J \exp\left[-\sum_K \frac{a_{KJ}\beta_I}{RT} - \left(\frac{G_J}{RT} + \ln p \right) \right] = 1, \tag{20}$$

where X_0 represents the molar concentration, a_{IJ} the number of elemental species I included in chemical species J, a_{KJ} the number of elemental species K included in chemical species J, β_I the negative chemical potential only when the system is in chemical equilibrium, R the gas constant, G_J the Gibbs free energy of chemical species J, p the pressure, and d_I the concentration of elemental species I.

When d_I and T were assigned as constraints, β_I and X_0 were obtained by solving the simultaneous nonlinear Equations (19) and (20). In this study, the computational code KINSOL (Collier et al., 2009) was used to solve these equations, and the concentration of each species at given T was obtainable by

$$X_J = X_0 \exp - \left[\sum_I \frac{a_{IJ}\beta_I}{RT} - \left(\frac{G_J}{RT} + \ln p \right) \right], \tag{21}$$

where X_J represents the molar concentration of chemical species J, and thermodynamic properties such as G_J and h_J were computed as functions of the temperature (Mcbride et al., 2002). According to this procedure, the concentration of the chemical species J at given T was acquired. However, the additional constraint that the enthalpy was constant before and after combustion was required so that the chemical equilibrium composition in combustion could be found. Thus, T must be found under the constraint

$$\sum_J h_J X_J = h_r, \tag{22}$$

where h_J represents the enthalpy of chemical species J, and h_r represents the enthalpy of reactants (before combustion). When we found T using Equation (22), the obtained results were the concentrations after combustion.
The equilibrium value Y_{Jeq} was obtained from reading the lookup table using $\tilde{Z}_H$, $\tilde{Z}_O$, $\tilde{Z}_N$, and $\tilde{h}_a$. Then, a simple multi-linear interpolation was used to extract information from the lookup table.

2.3 NO prediction using the extended Zeldovich mechanism

FLUENT version 13.0 has a function for computing the amount of the thermal NO_X using the extended Zeldovich mechanism as

$$O + N_2 \Leftrightarrow NO + N, \tag{23}$$

$$N + O_2 \Leftrightarrow O + NO, \tag{24}$$

$$N + OH \Leftrightarrow H + NO. \tag{25}$$

Because we used the basic function in FLUENT, we describe only the outline of the method to estimate the amount of NO here (Warnatz et al., 2006; Ansys, Inc, 2010). The reaction rate constants used in FLUENT were selected based on the evaluation of Hanson and Salimian (Hanson et al., 1984). To calculate the NO concentration in turbulence combustion, the time-averaged formation rate of NO must be computed at each computational cell. Methods of modeling the mean turbulent reaction rate of NO can be based on the presumed PDF model (Peng et al., 2009). FLUENT adopted the PDF model to predict the mass fraction of NO, and the reaction rate of the NO was expressed as

$$\bar{w}_{NO} = \int w_{NO} P(\phi_1) d\phi_1, \tag{26}$$

alternately, the PDF was related to two variables:

$$\bar{w}_{NO} = \iint w_{NO} P(\phi_1, \phi_2) d\phi_1 d\phi_2, \tag{27}$$

where w_{NO} represents the instantaneous reaction rate of NO, and $P(\phi_1)$ and $P(\phi_1, \phi_2)$ represent the PDFs of the variables. In this study, the mass fraction of O_2 and T were chosen as ϕ_1 and ϕ_2, respectively. As shown in Equations (23)–(25), the extended Zeldovich mechanism includes intermediate species such as O, N, H, and OH. The mass fractions of these species can be obtained by using the proposed technique. Thus, only the reaction rate of NO was computed by the presumed PDF model, while those of the intermediate species were taken into account using the proposed technique.

2.4 Numerical conditions

A H_2-air non-premixed flame was simulated to verify the accuracy of the proposed technique. The numerical conditions were based on Barrow's experimental data (Barrow et al., 2003a). Figure 2 shows the sketch of the computational domain used in this study. $\tilde{Y}_{H_2}$

in the fuel was 1.0; $\tilde{Y}_{O_2}$, $\tilde{Y}_{N_2}$, and $\tilde{Y}_{H_2O}$ in air were 0.231, 0.761, and 0.00720, respectively. Since $\tilde{Y}_{O_2}$, $\tilde{Y}_{N_2}$, and $\tilde{Y}_{H_2O}$ belong to group b, $\tilde{Z}_H = 0.008$, $\tilde{Z}_O = 0.23772$, and $\tilde{Z}_N = 0.76148$ were assigned in air. The fuel was injected from a nozzle with a radius of 3.75 mm. The velocity of the fuel and ambient air were 296 and 1.0 m/s, respectively. The temperature of the fuel and ambient air was set to 300 K. In all cases, a second-order upwind difference was applied to the governing equations of the momentum, mass fraction of chemical species J and elemental species I, and the energy equation. The two-dimensional axisymmetric solver in FLUENT was chosen using the axis indicated by the centerline in Fig. 2. The Reynolds stress model was chosen as the turbulence model; $C_{2\epsilon} = 1.80$, $\sigma_h = 0.7$, and $\sigma_m = 0.7$ of the model parameters were used to adjust the axial profile of the mixture fraction of the experimental data. In this study, the detailed chemical mechanism of H_2 suggested by Barrow (Barrow et al., 1999) was used to compute the reaction rates of the modified species in the proposed technique, and those of the chemical species taken into account by the EDC model.

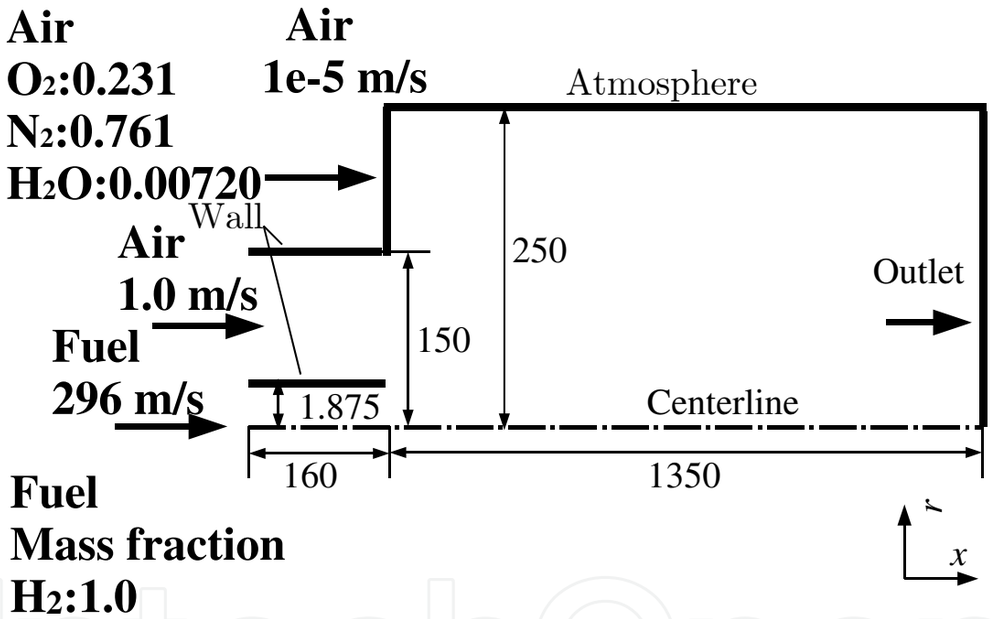

Fig. 2. Sketch of computational domain

3. Results

3.1 Prediction of mixture fraction, temperature, and mole fraction

First, to validate the prediction accuracy of the proposed technique, we compared the obtained results with those of the EDC model and the experiment. The lookup table was prepared before the combustion simulation, and it included the following species: H_2, O_2, H_2O, O, H, OH, HO_2, H_2O_2, NO, HNO, N_2O, N, NO_2, and N_2. In Figs. 3–18, x represents the axial distance from the exit of the nozzle; r, the radial distance from the centerline of the nozzle; L, the approximate visible flame length, which is equal to 675 mm in this flame; D, the diameter of the nozzle, which is equal to 3.75 mm in this flame; T, the temperature; EXP, the experimental data; EDC, the computational data predicted by the EDC model with

Barrow's detailed mechanism (Barrow et al., 1999); and $A_{H_2} = 100$, the computational data obtained by the proposed technique with $A_{H_2} = 100$. Although $A_{H_2} = 100$ was seemingly large, choosing this value means that H_2 is mixed with O_2 and is immediately consumed.

Fig. 3 shows the axial profile of the mixture fraction. Because the parameters $C_{2\epsilon} = 1.80$, $\sigma_h = 0.7$, and $\sigma_h = 0.7$ of the Reynolds stress model were chosen to match the axial mixture fraction obtained by the experiment, the computational results were close to the experimental data at $0.2 < x / L$. However, as shown in Fig. 3, those at $x / L < 0.2$ were slightly smaller than the experimental data. The mixture fraction was related to mass diffusion, which in turn depended on turbulence models. It can be seen from this result that mass diffusion was not similar to the experimental data at $x / L < 0.2$ (near the nozzle), and the turbulence model would have to be modified to obtain the closer result. However, the objective in this section is to confirm the validity of the proposed technique. To that end, we performed the simulation using the EDC model for reference. The EDC model has been widely applied to the simulation of combustion equipment (Stefanidis et al., 2006; Minotti et al., 2010), and the results obtained using the EDC model have been considered to be reliable for the engineered approach. The prediction of the proposed technique must approach that of the EDC model, because the expression of the reaction rate in the proposed technique was based on the EDC model.

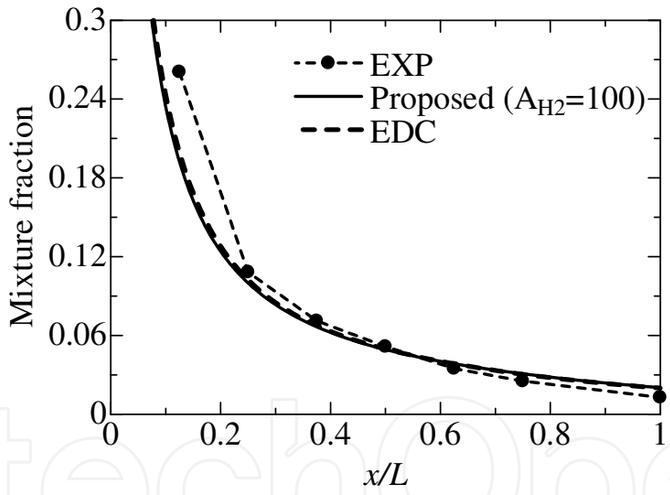

Fig. 3. Axial mixture fraction

The axial temperature T and mole fraction of H_2O are shown in Fig. 4. The mixture fractions of the computational results are in good agreement with each other, although those at $0.6 < x / L$ were slightly larger than the experimental data.

Fig. 5 shows the axial mole fraction of H_2 and O_2. Both the computational results of H_2 and O_2 were lower than those of the experimental data. It was found that the simulations slightly overestimated the consumption of H_2 and O_2 as compared with those of the experiment. The mole fraction of H_2 at $0.3 < x / L < 0.6$ obtained by the proposed technique was slightly larger than that of the EDC model. The reaction rate of H_2 was determined by the overall reaction, choosing $A_{H_2} = 100$ in the case of the proposed technique; the rate was computed

from the Barrow's detailed mechanism in the case of the EDC model. The overall reaction with choosing $A_{H_2} = 100$ in the proposed technique caused the difference of H_2 at $0.3 < x / L < 0.6$.

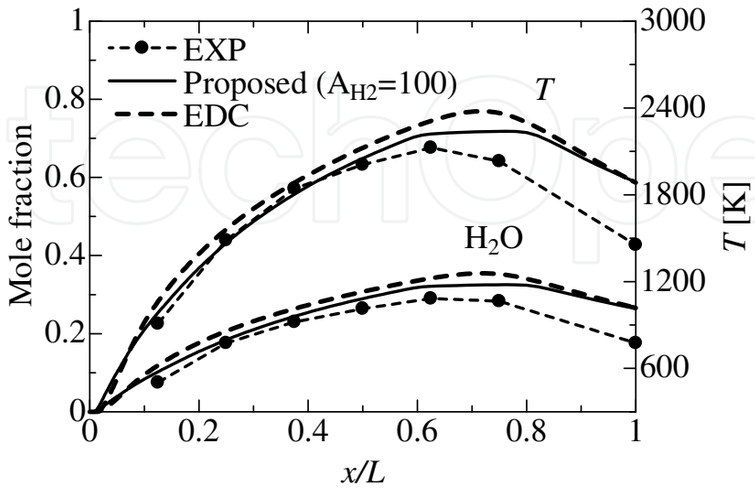

Fig. 4. Axial temperature T and mole fraction of H_2O

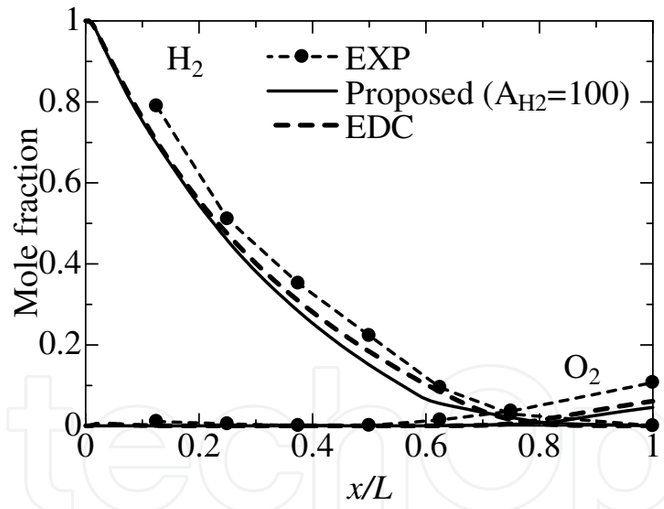

Fig. 5. Radial temperature and mole fraction of H_2 and O_2

The mole fraction of OH is plotted in Fig. 6. Generally, reaction equations including OH are needed to obtain the mole fraction of OH, but it was not required in the proposed technique. (However, the reaction equation of OH can be taken into account in the proposed technique using Equations (15)–(16) to improve the prediction accuracy.)

As shown in Fig. 6, the result of OH was comparatively small as compared with major species such as H_2, O_2, and H_2O; the amount of the radical species, such as H, O, and OH, were generally very subtle. For this reason, it was important to estimate the tendency of yield and consumption of the mole fraction of OH. In Fig. 6, the coordinates of the peaks of the mole fraction of OH obtained by the simulations were similar to the experimental data,

and we found that the mole fraction of OH obtained using the proposed technique was qualitatively similar to that obtained by the EDC model and experimental data.

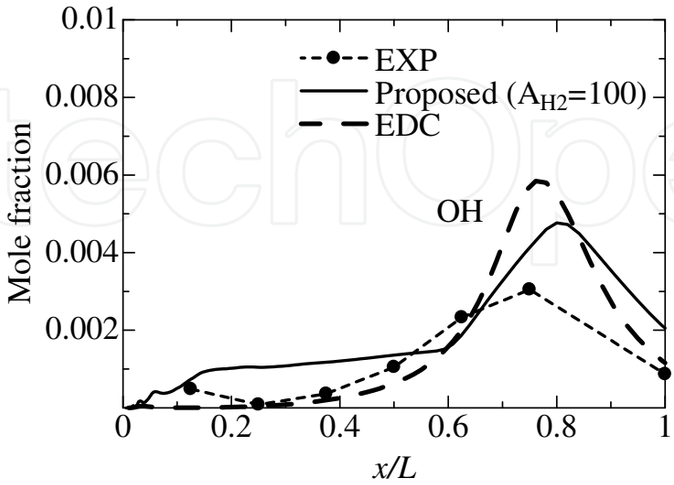

Fig. 6. Radial temperature and mole fraction of OH

Fig. 7 shows the radial mixture fraction at $x/L = 1/8$. Although the results obtained by the EDC model and the proposed technique were in good agreement, they were not close to the experimental data. As mentioned above, the difference of the mixture fraction between the simulations and experiment was related to the turbulence model, and not to either the EDC model or the proposed technique.

As we can observe from Fig. 8, the peaks of the temperature and the mole fraction of H_2O predicted with the use of the EDC and proposed models were at approximately $r/D = 4$, while that of the experimental data was at approximately $r/D = 2.9$. The deference of coordinates of the peaks between the simulation data and the experimental data derived mainly from turbulence model accuracy.

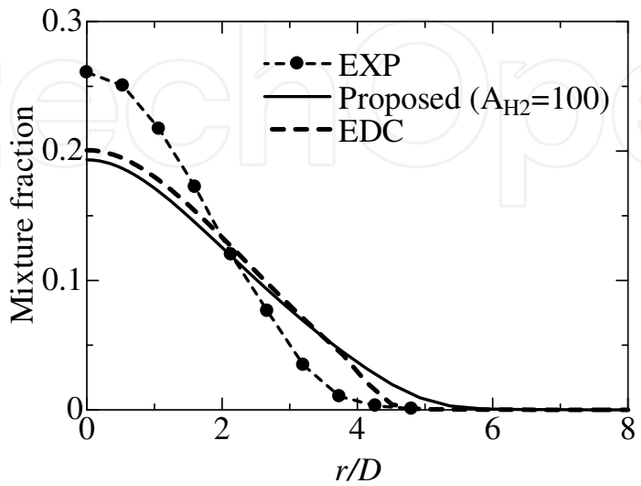

Fig. 7. Radial mixture fraction at $x/L = 1/8$

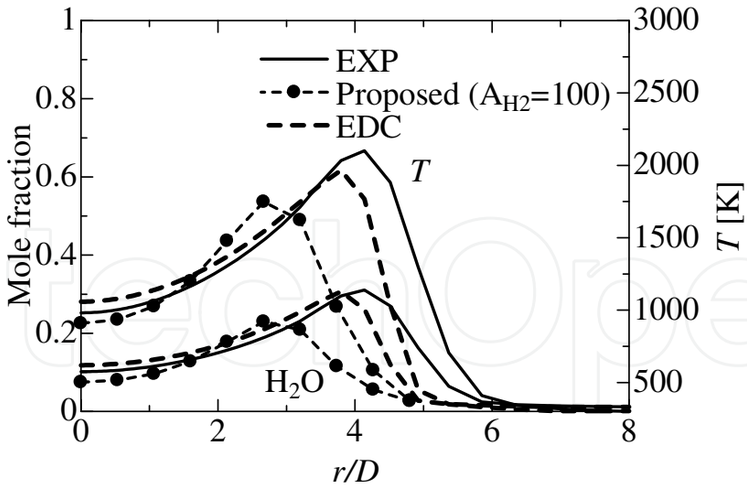

Fig. 8. Radial temperature and mole fraction of H_2O at $x/L = 1/8$

Fig. 9 shows the radial mole fraction of H_2 and O_2. The mole fraction of O_2 obtained by the proposed technique was lower than that predicted by the EDC model. In the proposed technique, the mole fraction of O_2 was obtained from the lookup table, which was prepared using the chemical equilibrium method. For this reason, consumption of O_2 was sometimes overestimated at points where the reaction was in the state of strong nonequilibrium.

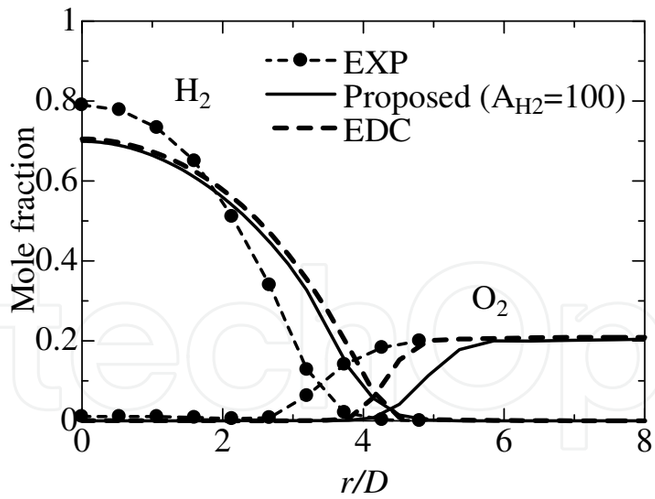

Fig. 9. Radial mole fraction of H_2 and O_2 at $x/L = 1/8$

As shown in Fig. 10, the coordinate values of the peak of the mole fraction of OH obtained by the simulations and experimental data are located at approximately $r/D = 4.1$ and $r/D = 2.7$, respectively. These values were slightly different from what was seen in the experiment. The coordinate of the peak mole fraction of OH was close to that of the mole fraction of H_2O and T. It can be seen from this tendency that OH was the indicative species of extinction and ignition phenomena.

The mixture fraction and temperature as well as mole fraction of H_2O are shown in Figs. 11 and 12, respectively. Both the computational data of the mixture fraction, temperature, and mole fraction of H_2O are in good agreement.

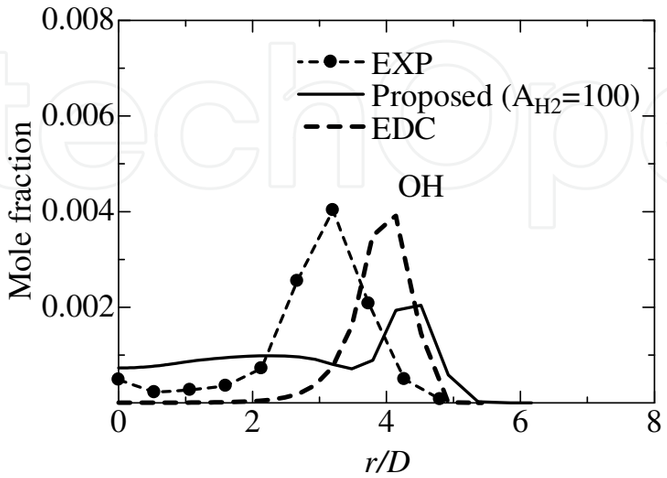

Fig. 10. Radial mole fraction of OH at x/L = 1/8

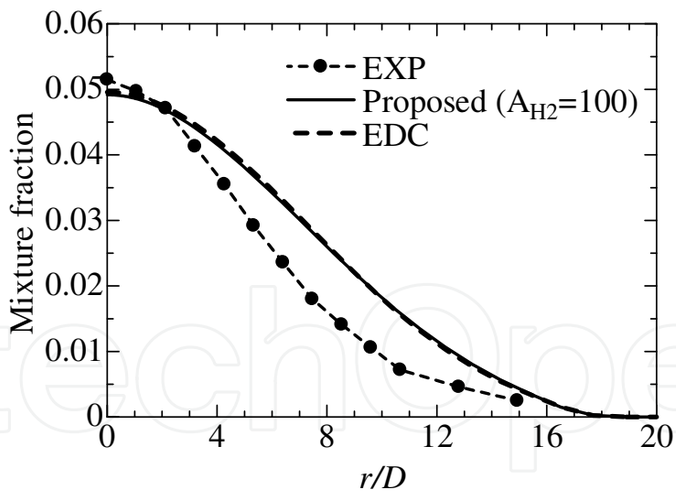

Fig. 11. Radial mixture fraction at $x/L = 1/2$

Fig. 13 shows the radial mole fraction of H_2 and O_2 at $x/L = 1/2$. Although the mole fractions of O_2 obtained by the proposed model and EDC model were almost similar, the result of H_2 computed using the proposed technique was not similar to that of the EDC model. This was because the proposed technique used $A_{H_2} = 100$ to estimate the reaction rate of H_2, while the reaction rate was computed using the detailed chemical mechanism in the EDC model. However, the difference of the results between the proposed technique and

EDC model were small as compared to the maximum mole fraction of H_2. Basically, the maximum mole fraction of H_2 was equal to 1.0 taken at $x/L=0$; the difference at $r/D=0.0$ between both computational results was about 0.03.

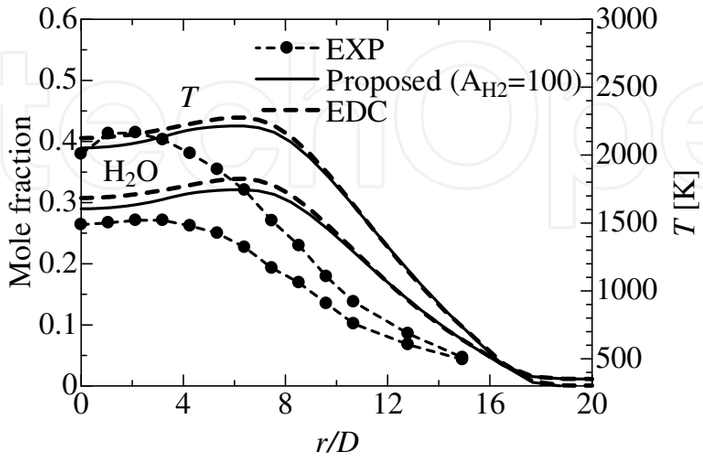

Fig. 12. Radial temperature and mole fraction of H_2O at x/L = 1/2

As shown in Fig. 14, the peaks of the mole fractions of OH obtained by the simulations and that of the experiment were located at approximately $r/D=7.6$ and $r/D=6.4$, respectively. The coordinates of the peaks obtained by the simulations were similar to each other, but they were slightly different from that of the experiment.

As shown in Figs. 15, 16, and 17, computational results for EDC and proposed models were in good agreement, but were either slightly greater or less than the experimental data, which showed a similar tendency to that of the other area, such as the radical direction at $x/L=1/8$ and $x/L=1/2$.

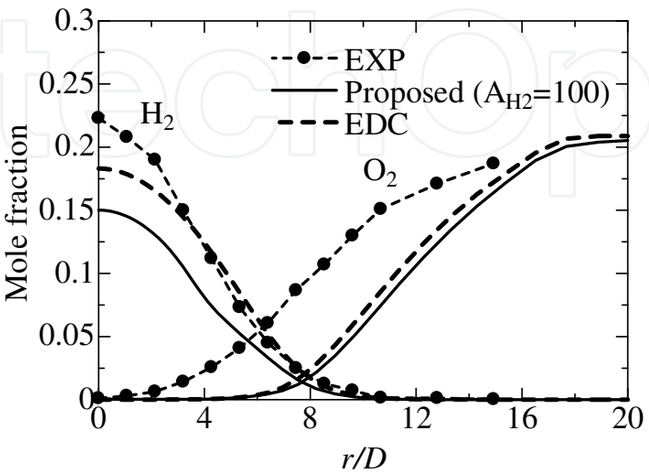

Fig. 13. Radial mole fraction of H_2 and O_2 at x/L = 1/2

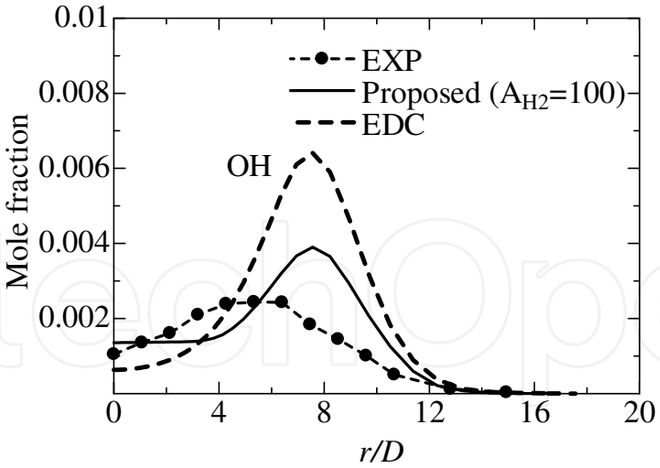

Fig. 14. Radial mole fraction of OH at $x/L = 1/2$

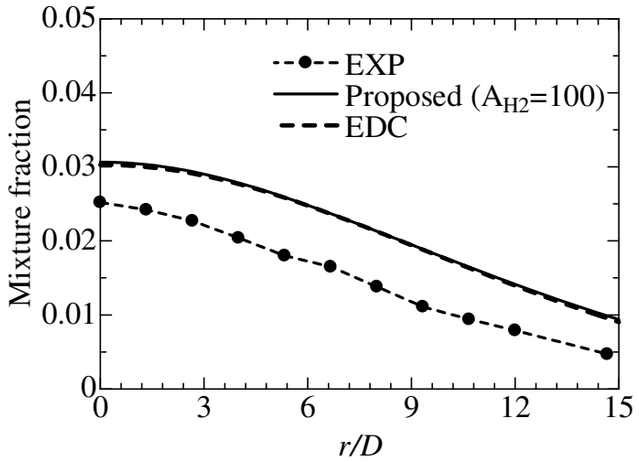

Fig. 15. Radial mixture fraction at $x/L = 3/4$

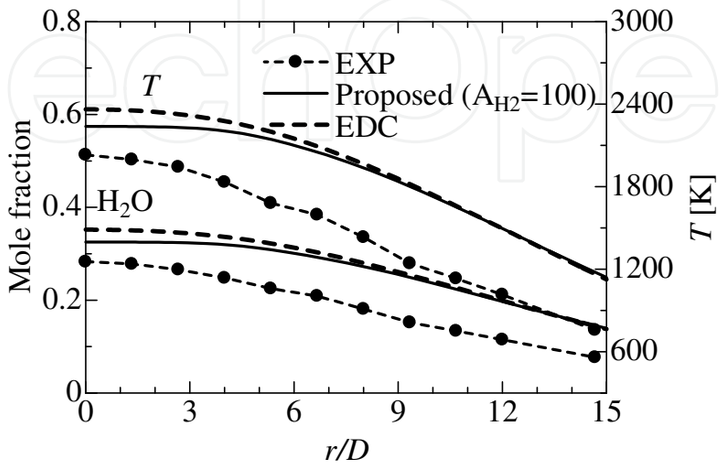

Fig. 16. Radial temperature and mole fraction of H_2O at $x/L = ¾$

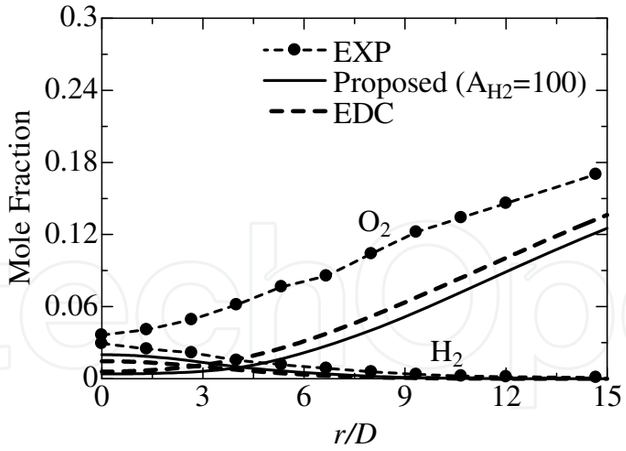

Fig. 17. Radial mole fraction of H_2 and O_2 at $x/L = 3/4$

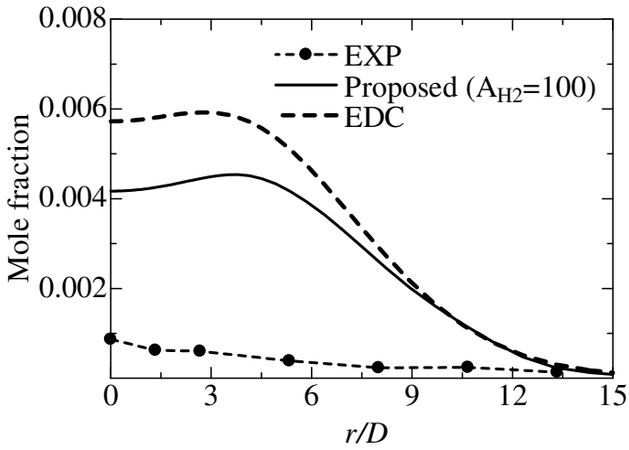

Fig. 18. Radial mole fraction of OH at $x/L = 3/4$

The radial mole fractions of OH at $x/L = 3/4$ are depicted in Fig. 18. The computational results were overestimated as compared with the experimental data, and the mole fraction of OH at $9 < r/D$ obtained using the proposed technique was similar to that obtained using the EDC model.

In this portion of the experiment, we found that the results of the mixture fraction, major species, and temperature obtained by the proposed technique were roughly similar to those predicted by the EDC model. The mole fraction of OH was not quantitatively similar to that of the EDC model; however, the coordinate values of the peaks of mole fraction of OH predicted by the proposed technique and EDC model were in good agreement with one another. Thus, the tendency of yield and consumption of OH was predicted with the proposed technique, which did not use the chemical equation of OH.

The computations show slight differences in the experimental data, even when the EDC model was applied to the combustion simulation. Moreover, we found that it is important to accurately predict the non-premixed flame using not only the combustion model but also the turbulence model. For this reason, further improvement of the combustion and turbulence models is a significant task for combustion simulation.

3.2 Prediction of NO

We show the application of the proposed technique to the simulation of NO in this section. In Figs. 19–30, "Proposed" indicates computational data obtained by the proposed technique with $A_{H_2} = 100$; "Proposed (H, O, OH)" indicates the computational data obtained by the proposed technique with $A_{H_2} = 100$ and reaction rates of H, O, and OH modified using Equations (15)–(16). Other symbols in Figs. 19–30 are as they were in the previous section. Two lookup tables were prepared before the combustion simulation. One table includes the species H_2, O_2, H_2O, O, H, OH, HO_2, H_2O_2, NO, HNO, N_2O, N, NO_2, and N_2; it was used for the case of the proposed technique with $A_{H_2} = 100$. The other table includes the species H_2, O_2, H_2O, HO_2, H_2O_2, NO, HNO, N_2O, N, NO_2, and N_2; it was prepared for the case of the proposed technique $A_{H_2} = 100$ and reaction rates of H, O, and OH modified using Equations (15)–(16).

As can be seen in Fig. 19, the peaks of the mole fraction of NO obtained by the simulation and that of the experiment were located at approximately $x / L = 0.82$. Those of the EDC model and proposed technique with modified reaction rates of H, O, and OH were bigger than the experimental data, while the peak obtained using the proposed technique without modified reaction rates was similar to that of the experiment. On the other hand, as shown in Fig. 20, the mole fraction of NO obtained by the proposed technique without the modified reaction rates was not similar to the experimental data. Thus, we did not determine which cases were most accurate in these simulations. As can be observed from Figs. 19 and 20, the amount of NO was very small as compared to the major species such as H_2, O_2, and H_2O. Therefore, the most important aim of the NO prediction was to simulate the tendency of yield and consumption of NO.

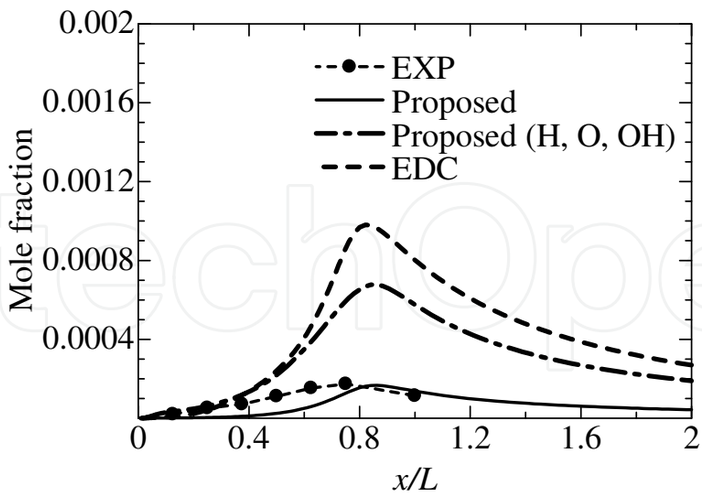

Fig. 19. Axial mole fraction of NO predicted with the extended Zeldovich mechanism

In Figs. 20 and 21, the coordinates of the peaks obtained by both the simulations were in good agreement. Moreover, as shown in Fig. 22, the peaks of the mole fractions were located at roughly $r / D = 6$, and the mole fraction of NO decreased at $6 < r / D < 15$.

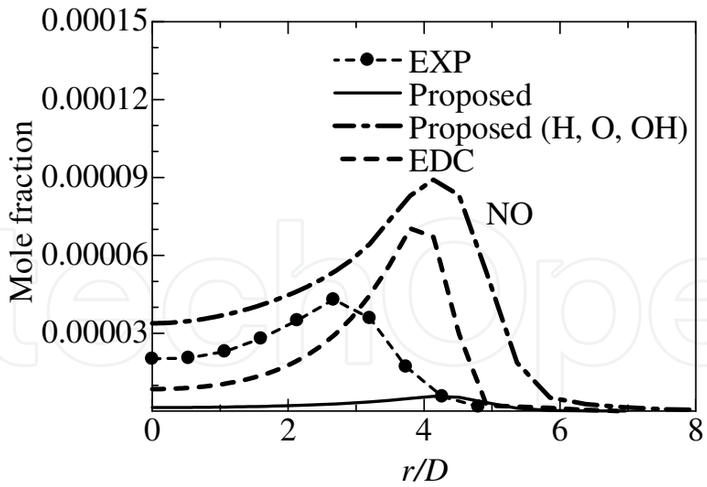

Fig. 20. Radial mole fraction of NO at x/L=1/8 predicted with the extended Zeldovich mechanism

It can be seen from Figs. 19–22 that the amounts of the NO prediction were not quantitatively correct; however, the peaks of the mole fractions obtained by the simulations were similar. Thus, we found that the tendency of yield and consumption of NO was simulated by all the cases in this part of the experiment.

The prediction accuracy of O is significant in the computation of the mass fraction of NO because the first reaction of the extended Zeldovich mechanism, expressed as $O + N_2 \rightarrow N + NO$, is the rate-limiting step (Warnatz et al., 2006). Thus, the amount of NO increases with an increase in O. As shown in Fig. 23, the axial mole fraction of O obtained using the proposed technique with modified reaction rates of H, O, and OH was larger than that of the EDC model.

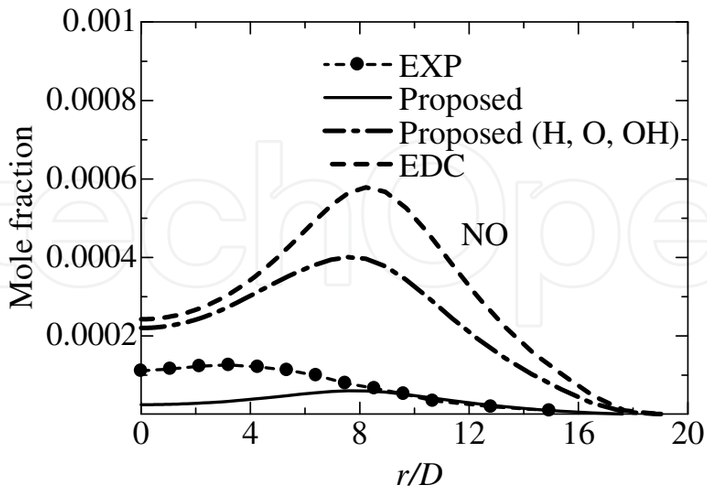

Fig. 21. Radial mole fraction of NO at x/L = 1/2

However, in Fig. 19, the axial mole fraction of NO obtained by the proposed technique with modified reaction rates of H, O, and OH was smaller than that of the EDC model. This was because axial T computed by the EDC model was overestimated as compared to that

computed by the proposed technique with modified reaction rates of H, O, and OH, as can be seen in Fig. 24. Thus, the first reaction of the extended Zeldovich mechanism became more reactive because of the increasing T of the EDC model.

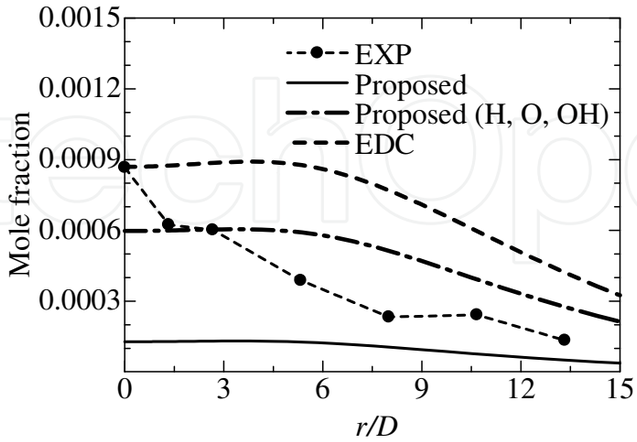

Fig. 22. Radial mole fraction of NO at $x/L = 3/4$

On the other hand, as can be seen in Figs. 25 and 26, either the mole fraction of O or T obtained using the proposed technique with modified reaction rates of H, O, and OH were larger than those of the EDC model. Therefore, the radial mole fraction of NO at $x/L = 1/8$ was also larger than that computed by the EDC model.

We found that the amount of NO was determined by the amount of O and T, and those of prediction accuracy were so important of obtaining the accurate mole fraction of NO. In the proposed technique, the reaction rates of the intermediate species such as H, O, and OH were computed, and the mole fractions can be obtained taking into account the chemical equations. Generally, when the reaction rates were modified using the chemical equations, the prediction accuracy of the chemical species was also increased (Fukumoto et al., 2010). However, even without the modified reaction rates, the proposed technique well simulated the mole fraction of O, and the improvement of the modified reaction rates was relatively small. Therefore, the computing the reaction rates of H, O, and OH can be omitted in this flame.

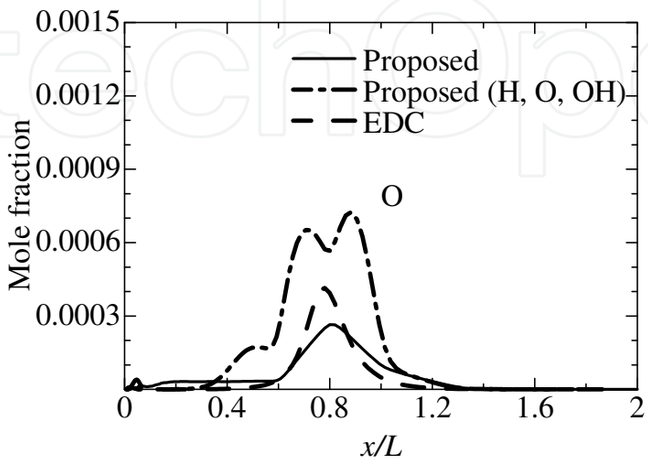

Fig. 23. Axial mole fraction of O

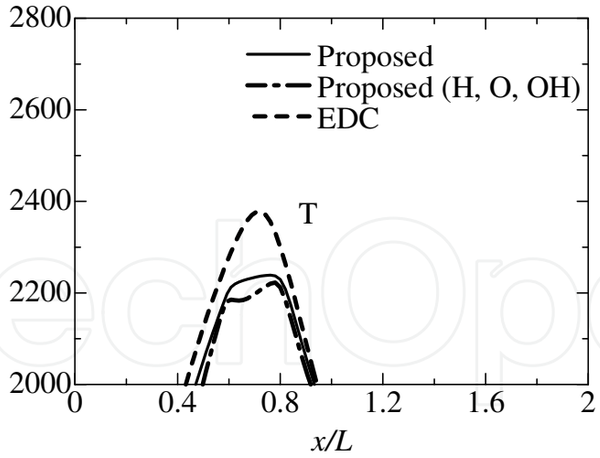

Fig. 24. Axial T ranging from 2000 K to 2800 K

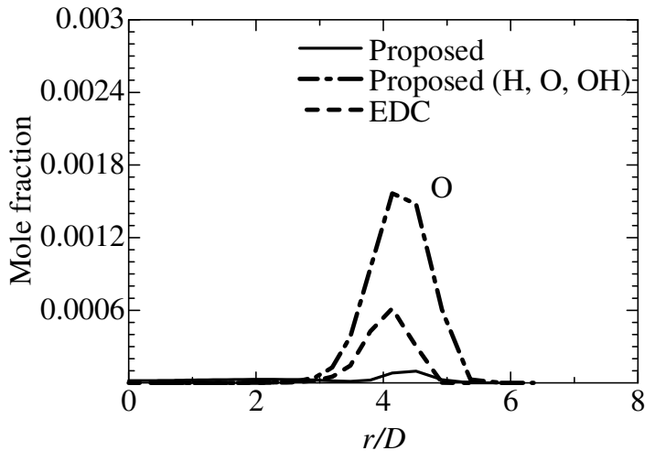

Fig. 25. Radial mole fraction of O at $x/L = 1/8$

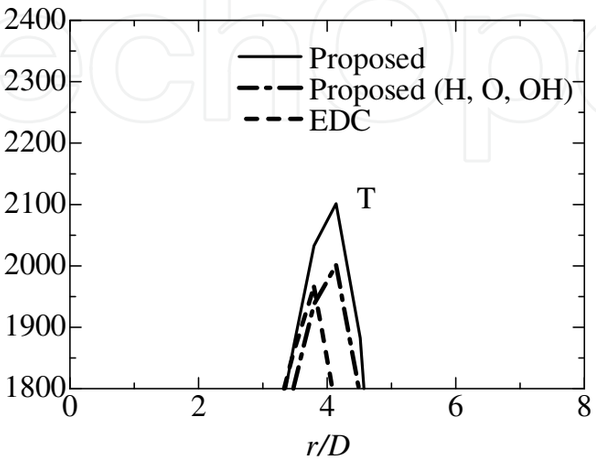

Fig. 26. Radial mole fraction of T at $x/L = 1/8$ ranging from 1800 K to 2400 K

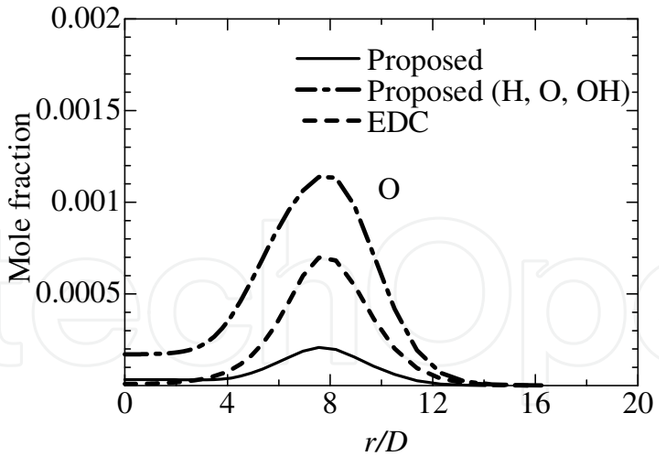

Fig. 27. Radial mole fraction of O at x/L=1/2

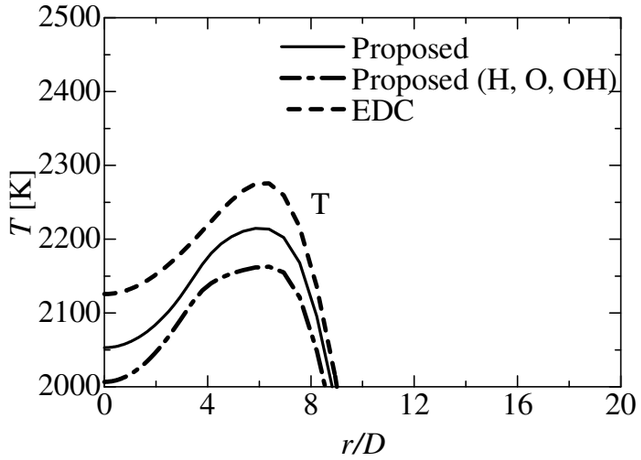

Fig. 28. Radial mole fraction of T at x/L=1/2 ranging from 2000 K to 2500 K

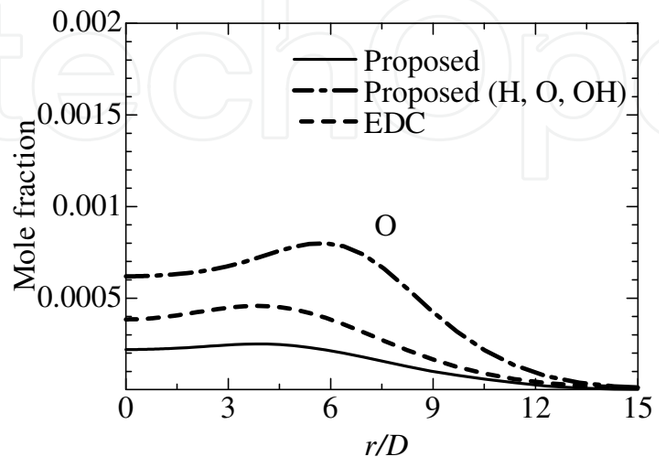

Fig. 29. Radial mole fraction of O at x/L=3/4

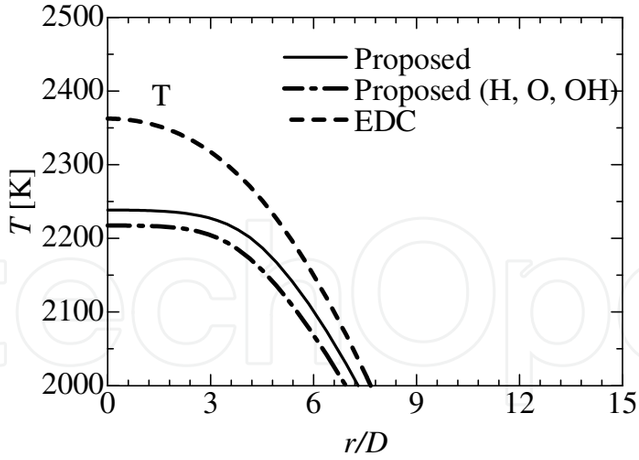

Fig. 30. Axial T at x/L=3/4 ranging from 2000 K to 2500 K

3.3 Influence of number of modified species and computational time

Due to the time required to compute reaction rates of these species, the computational time is dependent on the number of the chemical species in group a. Our proposed technique enables the shortening of these computational times. The purpose of this section is to discuss the prediction accuracy for the minor species and computational time required by the proposed technique. The numerical condition of the EDC model conformed to that presented in the previous sections, and the other two cases of the proposed technique were performed in this part of the experiment. In the first case of the proposed technique, the reaction rate of H_2 was computed by the estimated by Equations (17)–(18). In the second case, those of H, O, and OH were modified, and the reaction rate of H_2 was estimated.

Fig. 31 shows a comparison of the computational time in the case of the EDC model and two cases of the proposed technique. Each computational time per iteration was measured after the solution was converged and was measured during the 100 iterations of performing the reaction calculation and reading the lookup table. The CPU used in these simulations was the Intel Core i7-980X Processor Extreme Edition with 12M Cache, and 3.33 GHz. GFORTRAN 4.4.4 was chosen as a compiler, and CVODE 2.6 (Hindmarsh et al., 2009) was adopted to solve the ODEs of the reaction calculation. As can be seen in Fig. 31, the computational times for the EDC model—the two proposed techniques with modified H, O, and OH (second case) and with no modified species (first case)—were 8.99 s, 2.83 s, and 0.04 s, respectively. We found that the lower the number of included modified species, the fewer were the demands on lower computational time. On the other hand, the prediction accuracy also depended on the number of modified species included. Therefore, when the proposed technique is used, the number of modified species should be determined according to the required prediction accuracy. In the proposed technique, the computational time required increased with an increase in the number of modified species. However, the proposed technique has an advantage: We only chose the modified species and then the reduced mechanism was automatically built from the detailed mechanism.

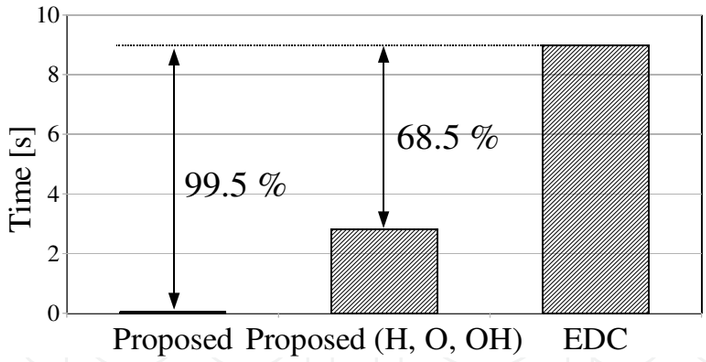

Fig. 31. Comparison of computational time

4. Conclusion

In this chapter, we presented a combustion simulation technique based on a chemical equilibrium method combined with the EDC model. The proposed technique makes it easy to construct a reduced mechanism according to the accuracy requirements of the chemical species, so that the computational time can be minimized.

We draw the following conclusions:

- The prediction accuracy of the proposed technique for the mixture fraction, major mole fraction, and *T* was similar to that of the EDC model.
- The coordinates of the peak OH mole fractions predicted by the proposed technique and EDC model were in good agreement. Thus, the tendency of yield and consumption of OH can be predicted using the proposed technique, which did not use the chemical equation of OH.
- The tendency of yield and consumption of NO was simulated by the proposed technique with the extended Zeldovich mechanism.
- A lower number modified species led to lower computational time. However, the prediction accuracy also relied on the number of modified species included. Modified species should be included according to the required prediction accuracy.

5. References

Amir, M. & Sadegh, T. (2010). Effect of Hydrogen on Hydrogen-Methane Turbulent Non-premixed Flame under MILD Condition. *Hydrogen Energy*, Vol. 35, No. 20, (October 2010), pp. 11324–11331, ISSN: 0360-3199

Ansys, Inc. (2011). Ansys FLUENT, (2010), Available from: http://www.ansys.com/

Ansys, Inc. (2010). *ANSYS FLUENT Theory Guide*, Ansys, Inc. Retrieved from http://www.ansys.com/

Barlow, R S. & Smith, N S A. (1999). Nitric Oxide Formation in Dilute Hydrogen Jet Flames: Isolation of the Effects of Radiation and Turbulence-Chemistry Submodels. *Combustion and Flame*, Vol. 117, No. 1, (April 1999), pp. 4–31, ISSN: 0010–2180

Barlow, R S. (2003a). Sandia H_2/He Flame Data-Release 2.0, In: *International Workshop on Measurement and Computation of Turbulent Non-premixed Flames*, June 2011, Available from: < http://www.sandia.gov/TNF/simplejet.html>

Barlow, R S. (2003b). Radiation Models, In: *International Workshop on Measurement and Computation of Turbulent Non-premixed Flames*, June 2011, Available from: < http://www.sandia.gov/TNF/radiation.html>

Collier, A M. & Hindmarsh, A C. (2009). KINSOL version 2.6.0, In: *SUNDIALS web site*, 30 June 2011, Available from https://computation.llnl.gov/casc/sundials/main.html/

Daniele, L M. (2009). Large Eddy Simulation of mixing and reaction in a Confined Impinging Jets Reactor. *Computers and Chemical Engineering*, Vol. 33, No. 2, (February 2009), pp. 393–534, ISSN: 0098-1354

Fukumoto, K. & Ogami, Y. (2010). Turbulent Diffusion Combustion Model using Chemical Equilibrium Combined with the Eddy Dissipation Concept for Reducing Detailed Chemical Mechanisms: An Application of H_2-air Turbulent Diffusion Flame. *Heat Transfer–Asian Research*, Vol. 39, No. 5, (July 2010), pp. 292–313, ISSN: 1523-1496

Fukumoto, K. & Ogami, Y. (2009). Simulation of CO-H_2-air Turbulent Diffusion Flame by the Combustion Model Combined Chemical Equilibrium Method with the Eddy Dissipation Concept Model. *Journal of High Temperature Society,* Vol. 39, No. 4, pp. 159-168, ISSN: 0387-1096

Gran, I R. & Magnussen, B F. (1996). A Numerical Study of a Bluff-body Stabilized Diffusion Flame. Part 2. Influence of Combustion Modeling and Finite-Rate Chemistry. *Combustion Science Technology,* Vol. 119, (1996), pp. (191–217), ISSN: 0010-2202

Hanson, R K. & Salimian S. (1984). Survey of Rate Constants in H/N/O Systems, *In*: *Combustion Chemistry*. Gardine, W C Jr, 36, Springer-Verlag, ISBN-10: 038790963X, ISBN-13: 978-0387909639, New York, USA

Hindmarsh, A C. & Serban, R. (11 May 2009). CVODE version 2.6.0, In: *SUNDIALS web site*, 30 June 2011, Available from: https://computation.llnl.gov/casc/sundials/main.html/

Magnussen, B F. (1989). Modeling of NO and Soot Formation by the Eddy Dissipation Concept, *Proceedings of 1st topic Oriented Technical Meeting*, Amsterdam, Netherlands, October 1989

Magnussen, B F. (2005). The Eddy Dissipation Concept: A Bridge Between Science and Technology, *Proceedings of ECCOMAS Thematic Conference on Computational Combustion,* Lisbon Portugal, June 2005

Mcbride, B J. & Zehe, M J. (2002). NASA Glenn Coefficients for Calculating Thermodynamic Properties of Individual Species. In: *NASA Technical Report TP-2002-211556*, 30 June 2011, Available from: http://gltrs.grc.nasa.gov/

Minotti, A. & Sciubba, E. (2010). LES of a Meso Combustion Chamber with a Detailed Chemistry, *Energies*, Vol. 3, No. 12, pp. 1943–1959, ISSN 1996–1073

Nagai, N. & Takagi, T. (15 December 2002). *JSME Combustion Handbook* (2nd edition), JSME, ISBN: 4-88898-074-8, Tokyo, Japan.

Ogami, Y. & Fukumoto, K. (2010). Simulation of Combustion by Vortex Method *Computer & Fluids*, Vol. 39, No. 4, (April 2010), pp. 592–603, ISSN: 0045-7930

Patankar, S. V. (1 January 1980). *Numerical Heat Transfer and Fluid Flow*. Taylor & Francis; ISBN-10: 0891165223, ISBN-13: 978-0891165224.

Peng, L. & Zhang, J. (2009). Simulation of Turbulent Combustion and NO Formation in a Swirl Combustor, *Chemical Engineering Science*, Vol. 64, No. 12, (June 2009), pp. 2903-2914, ISSN: 0009-2509

Stefanidis, G D. & Merci, B. (2006). CFD Simulations of Steam Cracking Furnaces using Detailed Combustion Mechanisms, *Computers & Chemical Engineering*, Vol. 30, No. 4, (15 February 2006), pp. 635–649, ISSN: 00981354

Warrants, J. & Maas, U. (2006). *Combustion* (4th edition), Springer-Verlag, ISBN-10: 3-540-25992-9, ISBN-13: 978-3-540-25992-3, Berlin, Germany

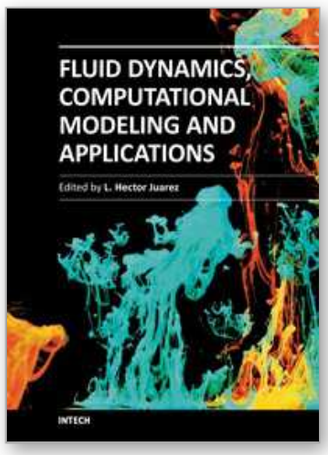

Fluid Dynamics, Computational Modeling and Applications

Edited by Dr. L. Hector Juarez

ISBN 978-953-51-0052-2
Hard cover, 660 pages
Publisher InTech
Published online 24, February, 2012
Published in print edition February, 2012

The content of this book covers several up-to-date topics in fluid dynamics, computational modeling and its applications, and it is intended to serve as a general reference for scientists, engineers, and graduate students. The book is comprised of 30 chapters divided into 5 parts, which include: winds, building and risk prevention; multiphase flow, structures and gases; heat transfer, combustion and energy; medical and biomechanical applications; and other important themes. This book also provides a comprehensive overview of computational fluid dynamics and applications, without excluding experimental and theoretical aspects.

InTech Europe
University Campus STeP Ri
Slavka Krautzeka 83/A
51000 Rijeka, Croatia
Phone: +385 (51) 770 447
Fax: +385 (51) 686 166
www.intechopen.com

InTech China
Unit 405, Office Block, Hotel Equatorial Shanghai
No.65, Yan An Road (West), Shanghai, 200040, China
中国上海市延安西路65号上海国际贵都大饭店办公楼405单元
Phone: +86-21-62489820
Fax: +86-21-62489821

IntechOpen